Communication

Ionic Conduction Mechanism and Design of Metal−Organic Framework Based Quasi-Solid-State Electrolytes

Tingzheng Hou,[#] Wentao Xu,[#] Xiaokun Pei, Lu Jiang, Omar M. Yaghi,* and Kristin A. Persson*

ACCESS | 📊 Metrics & More | 📖 Article Recommendations | 🆘 Supporting Information

ABSTRACT: We report the theoretical and experimental investigation of two polyoxometalate-based metal−organic frameworks (MOFs), $[(MnMo_6)_2(TFPM)]_{imine}$ and $[(AlMo_6)_2(TFPM)]_{imine}$, as quasi-solid-state electrolytes. Classical molecular dynamics coupled with quantum chemistry and grand canonical Monte Carlo are utilized to model the corresponding diffusion and ionic conduction in the two materials. Using different approximate levels of ion diffusion behavior, the primary ionic conduction mechanism was identified as solvent-assisted hopping (>77%). Detailed static and dynamic solvation structures were obtained to interpret Li$^+$ motion with high spatial and temporal resolution. A rationally designed noninterpenetrating MOF-688(one-fold) material is proposed to achieve 6−8 times better performance (1.6−1.7 mS cm^{-1}) than the current state-of-the-art (0.19−0.35 mS cm^{-1}).

Solid-state electrolytes with high mechanical strength and ionic conductivity are anticipated to revolutionize the energy storage industry.[1−5] This is due to their significant contributions to improved safety, low-temperature performance, and volumetric energy density as compared to conventional liquid electrolytes. Recently, anionic metal−organic frameworks (MOFs) with superior ionic conductivity and Li$^+$ transference numbers have opened a new avenue in the development of quasi-solid-state electrolytes (QSSEs).[6−11] To immobilize anions on the backbone of these frameworks, one approach is to directly link negatively charged building blocks, whereby the lithium counterions are introduced as the only mobile species inside the material.[9] For example, a three-fold interpenetrating anionic MOF (MOF-688) was synthesized from Anderson type polyoxometalate (POM) [N-$(C_4H_9)_4$]$_3$[MnMo$_6$O$_{18}${(OCH$_2$)$_3$CNH$_2$}$_2$] (MnMo$_6$) and tetrakis(4-formylphenyl)methane (TFPM) building units through imine condensation.[12] With propylene carbonate (PC) filling the pores, Li$^+$-exchanged MOF-688 exhibited a high ionic conductivity of 4.0×10^{-4} S cm^{-1} and high Li$^+$ transference number of 0.87 at 298 K.

In this new class of promising prototype QSSEs, it is important to understand the transport and conduction mechanisms, especially given the characterization challenges associated with transport measurements.[13−15] Solid-state nuclear magnetic resonance characterizations have shown that Li$^+$ transport in the framework channels involves complex interactions between cations, anions, and framework segments[16] and may exhibit a change in conduction mechanism with varying temperature.[17] Moreover, given the vast materials space that results from linking inorganic nodes and organic ligands,[18] it is important to develop theoretical methods that can predict and optimize the transport properties of MOFs to support the experimental efforts.[9] Yuan et al.[19] computed the energetics of Li$^+$ hopping between binding sites in Cu-MOF-74, which provides support for a hypnotized hopping

mechanism of Li$^+$ conduction.[8] However, the detailed ionic transport mechanisms and how exactly the anionic species and solvent molecules cooperatively facilitate the Li$^+$ diffusion are still unclear.[9]

Classical molecular dynamics (MD) simulations have shown excellent results in modeling the solvation and transport properties of liquid electrolytes[20,21] as well as the diffusion and adsorption properties of MOFs,[22,23] and have been considered as a promising tool to provide in-depth understanding of MOF-related QSSEs.[9] In this contribution, by combining MD simulations with quantum chemistry and grand canonical Monte Carlo (GCMC), we identified solvent-assisted hopping as the dominant pathway for Li$^+$ conduction in MOF-688 materials, revealing the critical role of the solvent in MOF-based QSSEs. This work constitutes the first theoretical model that accurately describes the ionic conduction mechanism of MOF-based QSSEs at an atomistic level, which is challenging to obtain from experimental results,[13,14] and provides guidance for possible improvements.

A molecular simulation model, denoted as MOF-688(Mn), was created from X-ray single crystal structure of MOF-688, $[(MnMo_6)_2(TFPM)]_{imine}$.[12] In parallel, an isoreticular structure $[(AlMo_6)_2(TFPM)]_{imine}$, termed MOF-688(Al), was synthesized and modeled by substituting Mn^{3+} with Al^{3+} to investigate the influence of the POM center metal ion on ionic conduction. Li$^+$ counterions were introduced in both MOFs with a POM/Li$^+$ ratio of 1:3 (Supporting Information (SI) Section 1). Hybrid MD and GCMC simulations[24] were

performed to equilibrate the content of PC solvent in the pores of MOFs. The obtained PC-infused structures with a POM/PC ratio of 16:170 and a Li⁺ concentration of 2.0 mol L⁻¹ were then utilized to perform MD simulations (SI Section 3). By analyzing MD trajectories over a few tens of nanoseconds, three different types of Li⁺ motion were observed (Scheme 1):

Scheme 1. Three Proposed Conduction Mechanisms for MOF-688

① Hopping on the same POM
② Hopping between POMs
③ Free diffusion

Li⁺ conduction mechanisms
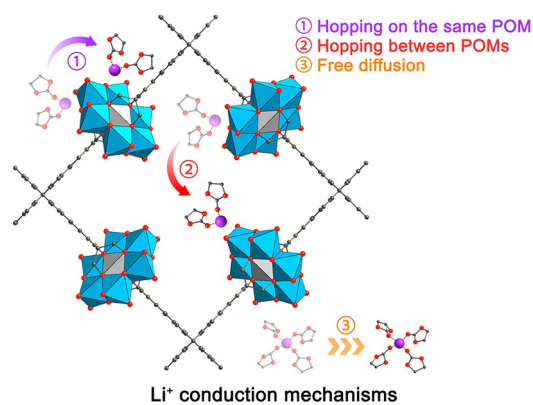
(1) Li⁺ hopping on the same POM cluster between the outmost oxygens (i.e., binding sites); (2) Li⁺ hopping between POM clusters; and (3) solvated Li⁺ diffusion, where Li⁺ is coordinated and separated only by PC that can freely diffuse in bulk solvent.

To identify the ionic conduction mechanism of the two model materials, we calculated the ionic conductivity using different levels of approximation (SI Section 5): first using rigorous Green−Kubo (GK) relations which account for intermolecular transport correlations, second using the dilute approximation Nernst−Einstein equation, and third, using a single-mechanism hopping model. Comparing results of the three models enabled us to conclusively determine the dominant conduction mechanisms of both materials.

The calculated GK conductivity of MOF-688(Mn) at 298 K (Figure 1c) and as a function of temperature (Figure S12) agree well with the experimental trend, validating that the molecular model is suitable for the quantitative study of transport phenomena of MOF-based QSSEs. Moreover, MOF-688(Al) exhibits a slightly lower ionic conductivity than MOF-688(Mn), while the difference is within the error range. This observation indicates that changing the type of center metal ions is unlikely to significantly affect ionic conductivity. In addition, the discrepancy of the solvation structure between the two model materials is minor (Figure 1a,b, Figure S7) and attributed to a slightly weaker interaction between Li⁺ and MnMo₆ (Table S2). It is further found that the self-diffusion coefficients of tethered and solvated Li⁺ are similar (Figure S10). Considering that only 7% Li⁺ are fully detached from the POMs in both MOFs and solvated (Figure 1a), the diffusion of solvated Li⁺ is excluded from the major conduction mechanism.

Next, we calculated the ionic conductivity assuming that the ionic conduction is mostly contributed by uncorrelated Li⁺ (self-)diffusion, and the intrinsically anionic frameworks are treated as fixed. With this assumption, the ionic conduction can be correlated to the self-diffusion coefficient of Li⁺ using the Nernst−Einstein (NE) equation. The computed NE conductivity is in fair agreement with the GK conductivity.
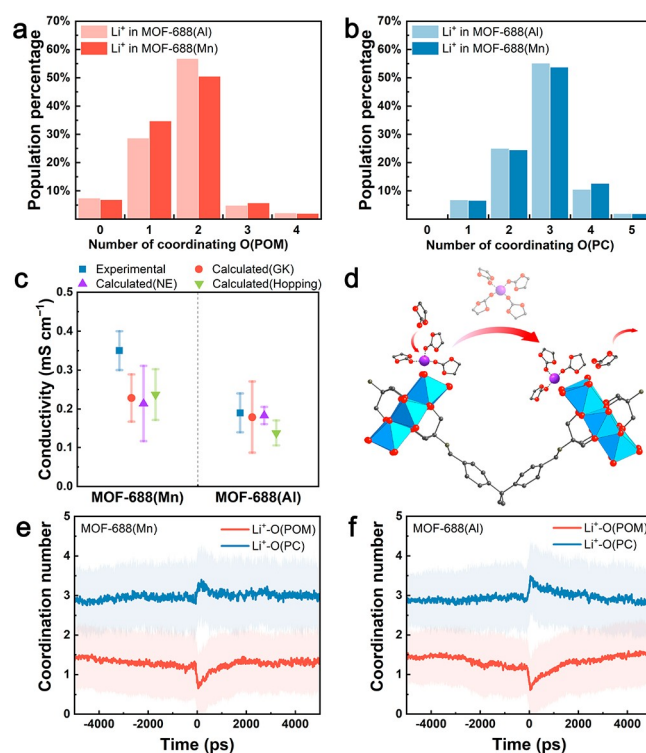

Figure 1. Conduction mechanism of MOF-688. The coordination number of (a) Li⁺-O(POM), and (b) Li⁺-O(PC) in MOF-688(Al) and MOF-688(Mn). (c) Ionic conductivities of MOF-688(Mn) and MOF-688(Al) from experimental measurements, and theoretical calculations using Green−Kubo relations (GK), Nernst−Einstein equation (NE), and simple hopping model (hopping). (d) Scheme of solvent-assisted hopping. The evolution of Li⁺-O(POM) and Li⁺-O(PC) coordination numbers before and after hopping in (e) MOF-688(Mn) and (f) MOF-688(Al). The light-colored area denotes the extent of standard deviation.

Additionally, the concerted/correlated ion diffusion observed in all-solid-state electrolytes (e.g., NASICON[25,26]) is insignificant in the MOF-based QSSE, as analyzed using the Onsager transport theory (SI Section 5). Hence, the underlying assumption arguably holds that the conductivity is mostly contributed by Li⁺ self-diffusion, in agreement with the measured transference number (t_{Li+}= 0.87).[12]

Finally, we calculated the ionic conductivity with a simple hopping model. The uncorrelated individual ion hopping can be described by a random-walk model.[27] By incorporating the hopping diffusion coefficient into the NE equation, we obtain the hopping conductivity. While the calculation utilizes a simplified model, it yielded fair agreement with the other two models. On average, the hopping conductivity contributes to 100% and 77% of the GK conductivity of MOF-688(Mn) and MOF-688(Al), respectively, suggesting that Li⁺ hopping between POM clusters dominates Li⁺ diffusion.

The evolution of Li⁺ solvation sheath during Li⁺ hopping further reveals the solvent effect on the process. We observed discrete changes of average coordination numbers of both O(PC) and O(POM) before and after each hopping event (set to 0 ps) (Figure 1e,f). During hopping, the coordination number between Li⁺ and O(POM) decreases as Li⁺ no longer binds to previous binding sites and has not reestablished binding with another POM. Simultaneously, the average coordination number of O(PC) increases from 3 to 3.5 for both MOF-688(Mn) and MOF-688(Al). In the following

500−1000 ps after hopping, when Li$^+$ is gradually tethered to the framework and the excess PC leaves the Li$^+$ solvation sheath, the coordination numbers of O(PC) and O(POM) are restored to the bulk average. The direct involvement of the excess PC suggests that the primary mechanism of Li$^+$ conduction is *solvent-assisted hopping* between POM clusters (Figure 1d), while the short residence time further indicates that the excess PC plays a temporary role rather than forming solvent-separated Li$^+$ solvation structures that diffuse freely.

We find that the local charge distribution on the POM surface largely determines the interaction between Li$^+$ and the framework. The electrostatic potential (ESP) surface of MnMo$_6$ (Figure 2a,b) and AlMo$_6$ (Figure S13) was calculated
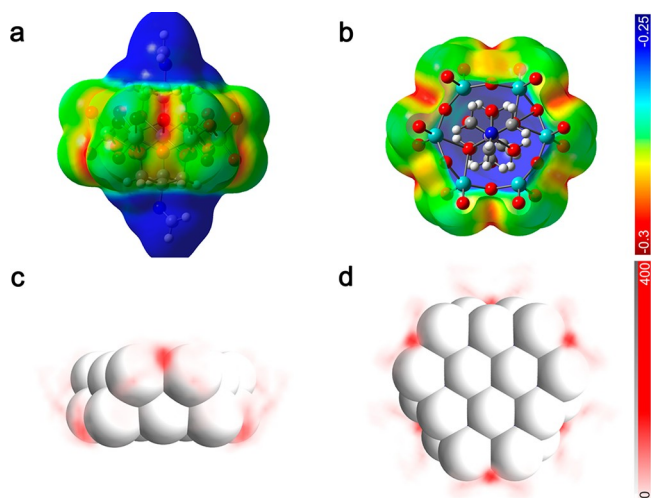

Figure 2. Charge and Li$^+$ distribution on MnMo$_6$ surface. (a) Front and (b) top view of the electrostatic potential (ESP) surface of MnMo$_6$. Carbon, hydrogen, oxygen, nitrogen, and molybdenum atoms are represented by gray, white, red, blue, and cyan, respectively. The color bar shows the electrostatic potential in volts. (c) Front and (d) top view of the Li$^+$ density plot on MnMo$_6$ surface. White balls denote the oxygens in MnMo$_6$. The color bar shows Li$^+$ number count from 100,000 randomly sampled coordinates.

as a measure of the Coulombic interaction between POM and Li$^+$. The ESP distribution of the two clusters is nearly identical, indicating that center metal ions with the same valency exhibit minor influence on the surface charge distribution of POM. The Li$^+$ density distribution around MnMo$_6$ (Figure 2c,d) coincides well with the ESP distribution, where the highest Li$^+$ density is found on sites between two adjacent MoO$_4$ moieties with the lowest electrostatic potential. This observation indicates that the electrostatic term is dominant in the interaction between Li$^+$ and MnMo$_6$, which further determines the most probable Li$^+$ binding sites. In addition, Li$^+$ can occasionally be monodentate-coordinated by one O as observed in the density plot.

The revealed correlation between the charge distribution and Li$^+$ distribution has important implications for the rational design of MOF-based QSSEs. Strongly localized charges that are immobilized on POM are expected to produce a tightly confined Li$^+$ distribution. The overbinding between Li$^+$ and the framework may lead to less favorable Li$^+$ hopping with decreased mobility and ionic conductivity. Therefore, we surmise that more distributed local charges on POM are expected to facilitate weaker binding with Li$^+$ and to enhance Li$^+$ motion.[7]

The solvent is another important factor regulating Coulombic interaction. In MOF-based QSSEs, the solvent screens Li$^+$ from the anionic frameworks, an aspect that results in less correlation between the Li$^+$ motion and the framework.[28] The apparent and effective Li$^+$ concentrations in MOF-688(Mn) are calculated to be 2.0 and 2.6 mol L^{-1}, respectively (SI Section 10).[29] The substantial Li$^+$/PC ratio (1:3.54) and corresponding Li$^+$ concentration suggest a high ionic strength in the material. The low PC content is mainly due to the limited pore volume resulting from the interpenetrating frameworks (Figure 3a). Therefore, we propose
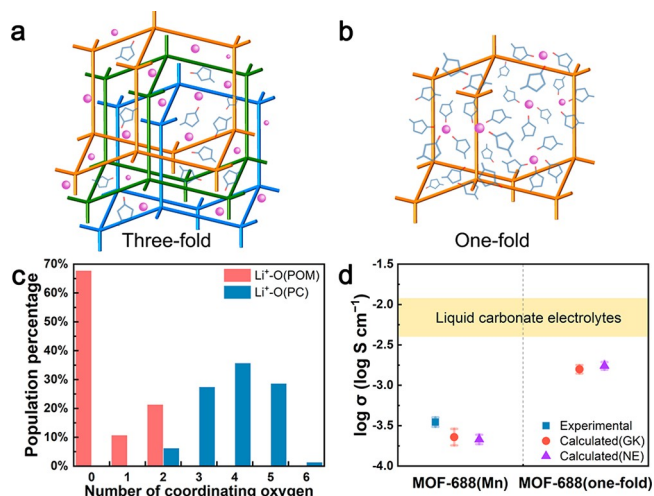

Figure 3. MOF-688(one-fold) design. Schemes of MOF-688 QSSEs with (a) three-fold and (b) proposed one-fold interpenetrating structures. (c) Coordination number of Li$^+$-O(POM) and Li$^+$-O(PC) in MOF-688(one-fold). (d) Comparison of ionic conductivities of MOF-688(Mn), MOF-688(one-fold), and the conductivity range of liquid carbonate electrolytes (highlighted).

that reducing the degree of interpenetration could be an effective approach to increase the pore volume and accordingly the amount of solvent in pores, thereby reducing the viscosity and ionic strength.

To corroborate the hypothesized design, we modeled a noninterpenetrating MOF-688 denoted as MOF-688(one-fold) (Figure 3b). After the same insertion process, a POM/PC ratio of 8:355 was obtained (Figure S6). The apparent and effective Li$^+$ concentrations are both 0.7 mol L^{-1}, comparable to the usual concentration (1.0 mol L^{-1}) of conventional liquid electrolytes. Further analysis of solvation structure reveals that more than 60% Li$^+$ are fully solvated by PC (Figure 3c, Figure S7). The boost in solvent-separated Li$^+$ is especially favorable for the uncorrelated Li$^+$ diffusion in electrolytes.[6] Using the same methods, the GK and NE conductivities of MOF-688(one-fold) are calculated to be 1.58 and 1.74 mS cm^{-1}, respectively. The theoretical prediction (Figure 3d) is almost an order of magnitude higher than the conductivity of MOF-688(Mn) and other anionic MOF-based electrolyte,[9,10] and significantly narrows the gap with typical liquid electrolyte conductivities (5−10 mS cm^{-1}).[30,31]

Furthermore, specific contributions from the tethered and solvated Li$^+$ to the total ionic conductivity were calculated using the NE equation and Li$^+$ self-diffusion coefficients (Figure S11), in which the solvated Li$^+$ contributed to 64% of the total ionic conductivity. Therefore, the ionic conduction in MOF-688(one-fold) can be mainly attributed to the solvated

Li$^+$ diffusion, providing a different ionic conduction mechanism with significantly improved conductivity. Moreover, unlike polymers which can become solvated and lose their mechanical strength after mixing with organic electrolyte,[32] mechanical properties of MOFs can even be enhanced when solvent fills the pores.[33,34] The bulk modulus (Voigt average) of MOF-688(one-fold) is calculated to be 1.1 and 2.4 GPa before and after adding PC, respectively. This is 1 to 2 orders of magnitude higher than that of poly(ethylene oxide) gel polymer electrolytes (a common QSSE)[35−37] and retained about 1/3 of the 3-fold interpenetrating MOF-688(Mn) (SI Section 7).

To actually synthesize MOF-688(one-fold) with a much larger pore size than MOF-688(Mn), large and appropriately matching template guests or cations are required to support the reticulation of organic and inorganic building blocks. We envision that screening methods based on first-principles calculations[38] and machine learning of suitable synthetic pathways[39,40] may help identify template candidates.

ASSOCIATED CONTENT

Supporting Information

The Supporting Information is available free of charge at https://pubs.acs.org/doi/10.1021/jacs.2c03710.

> Experimental and computational details including materials and synthetic procedures, single-crystal X-ray analysis, molecular dynamics and grand canonical Monte Carlo simulations, coordination analysis, conductivity calculation, elastic constants calculation, electrostatic potential surface analysis, and concentration analysis. (PDF)

Accession Codes

CCDC 2165003 contains the supplementary crystallographic data for this paper. These data can be obtained free of charge via www.ccdc.cam.ac.uk/data_request/cif, or by emailing data_request@ccdc.cam.ac.uk, or by contacting The Cambridge Crystallographic Data Centre, 12 Union Road, Cambridge CB2 1EZ, UK; fax: +44 1223 336033.

AUTHOR INFORMATION

Corresponding Authors

Omar M. Yaghi − *Department of Chemistry, University of California, Berkeley, California 94720, United States;* orcid.org/0000-0002-5611-3325; Email: yaghi@berkeley.edu

Kristin A. Persson − *Department of Materials Science and Engineering, University of California, Berkeley, California 94720, United States; The Molecular Foundry, Lawrence Berkeley National Laboratory, Berkeley, California 94720, United States;* orcid.org/0000-0003-2495-5509; Email: kapersson@lbl.gov

Authors

Tingzheng Hou − *Department of Materials Science and Engineering, University of California, Berkeley, California 94720, United States; Energy Technologies Area, Lawrence Berkeley National Laboratory, Berkeley, California 94720, United States;* orcid.org/0000-0002-7163-2561

Wentao Xu − *Department of Chemistry, University of California, Berkeley, California 94720, United States;* orcid.org/0000-0002-9772-1036

Xiaokun Pei − *Department of Chemistry, University of California, Berkeley, California 94720, United States;* orcid.org/0000-0002-6074-1463

Lu Jiang − *Department of Materials Science and Engineering, University of California, Berkeley, California 94720, United States; Materials Sciences Division, Lawrence Berkeley National Laboratory, Berkeley, California 94720, United States;* orcid.org/0000-0001-8103-4912

Complete contact information is available at:
https://pubs.acs.org/10.1021/jacs.2c03710

Author Contributions

#T.H. and W.X. contributed equally.

Notes

The authors declare no competing financial interest.

REFERENCES

(1) Chen, R.; Qu, W.; Guo, X.; Li, L.; Wu, F. The pursuit of solid-state electrolytes for lithium batteries: from comprehensive insight to emerging horizons. *Mater. Horiz.* **2016**, *3*, 487−516.

(2) Lin, D.; Liu, Y.; Cui, Y. Reviving the lithium metal anode for high-energy batteries. *Nat. Nanotechnol.* **2017**, *12*, 194−206.

(3) Fan, L.; Wei, S.; Li, S.; Li, Q.; Lu, Y. Recent Progress of the Solid-State Electrolytes for High-Energy Metal-Based Batteries. *Adv. Energy Mater.* **2018**, *8*, 1702657.

(4) Cheng, X.-B.; Zhao, C.-Z.; Yao, Y.-X.; Liu, H.; Zhang, Q. Recent Advances in Energy Chemistry between Solid-State Electrolyte and Safe Lithium-Metal Anodes. *Chem.* **2019**, *5*, 74−96.

(5) Qin, K.; Holguin, K.; Mohammadiroudbari, M.; Huang, J.; Kim, E. Y. S.; Hall, R.; Luo, C. Strategies in Structure and Electrolyte Design for High-Performance Lithium Metal Batteries. *Adv. Funct. Mater.* **2021**, *31*, 2009694.

(6) Miner, E. M.; Dinca, M. Metal- and covalent-organic frameworks as solid-state electrolytes for metal-ion batteries. *Philos. Trans. R. Soc. A* **2019**, *377*, 20180225.

(7) Park, S. S.; Tulchinsky, Y.; Dinca, M. Single-Ion Li$^+$, Na$^+$, and Mg^{2+} Solid Electrolytes Supported by a Mesoporous Anionic Cu-Azolate Metal-Organic Framework. *J. Am. Chem. Soc.* **2017**, *139*, 13260−13263.

(8) Wiers, B. M.; Foo, M. L.; Balsara, N. P.; Long, J. R. A solid lithium electrolyte via addition of lithium isopropoxide to a metal-organic framework with open metal sites. *J. Am. Chem. Soc.* **2011**, *133*, 14522−5.

(9) Zhao, R.; Wu, Y.; Liang, Z.; Gao, L.; Xia, W.; Zhao, Y.; Zou, R. Metal−organic frameworks for solid-state electrolytes. *Energy Env. Sci.* **2020**, *13*, 2386−2403.

(10) Huang, W.-H.; Li, X.-M.; Yang, X.-F.; Zhang, X.-X.; Wang, H.-H.; Wang, H. The recent progress and perspectives on metal- and

covalent-organic framework based solid-state electrolytes for lithium-ion batteries. *Mater. Chem. Front.* **2021**, *5*, 3593−3613.

(11) Judez, X.; Martinez-Ibañez, M.; Santiago, A.; Armand, M.; Zhang, H.; Li, C. Quasi-solid-state electrolytes for lithium sulfur batteries: Advances and perspectives. *J. Power Sources* **2019**, *438*, 226985.

(12) Xu, W.; Pei, X.; Diercks, C. S.; Lyu, H.; Ji, Z.; Yaghi, O. M. A Metal-Organic Framework of Organic Vertices and Polyoxometalate Linkers as a Solid-State Electrolyte. *J. Am. Chem. Soc.* **2019**, *141*, 17522−17526.

(13) Fong, K. D.; Self, J.; Diederichsen, K. M.; Wood, B. M.; McCloskey, B. D.; Persson, K. A. Ion Transport and the True Transference Number in Nonaqueous Polyelectrolyte Solutions for Lithium Ion Batteries. *ACS Cent. Sci.* **2019**, *5*, 1250−1260.

(14) Cronau, M.; Szabo, M.; König, C.; Wassermann, T. B.; Roling, B. How to Measure a Reliable Ionic Conductivity? The Stack Pressure Dilemma of Microcrystalline Sulfide-Based Solid Electrolytes. *ACS Energy Lett.* **2021**, *6*, 3072−3077.

(15) Winand, J. M.; Depireux, J. Measurement of Ionic Conductivity in Solid Electrolytes. *Europhys. Lett.* **1989**, *8*, 447−452.

(16) Brus, J.; Czernek, J.; Urbanova, M.; Rohlicek, J.; Plechacek, T. Transferring Lithium Ions in the Nanochannels of Flexible Metal-Organic Frameworks Featuring Superchaotropic Metallacarborane Guests: Mechanism of Ionic Conductivity at Atomic Resolution. *ACS Appl. Mater. Interfaces* **2020**, *12*, 47447−47456.

(17) Zettl, R.; Lunghammer, S.; Gadermaier, B.; Boulaoued, A.; Johansson, P.; Wilkening, H. M. R.; Hanzu, I. High Li^+ and Na^+ Conductivity in New Hybrid Solid Electrolytes based on the Porous MIL-121 Metal Organic Framework. *Adv. Energy Mater.* **2021**, *11*, 2003542.

(18) Dzubak, A. L.; Lin, L. C.; Kim, J.; Swisher, J. A.; Poloni, R.; Maximoff, S. N.; Smit, B.; Gagliardi, L. Ab initio carbon capture in open-site metal-organic frameworks. *Nat. Chem.* **2012**, *4*, 810−6.

(19) Yuan, S.; Bao, J. L.; Wei, J.; Xia, Y.; Truhlar, D. G.; Wang, Y. A versatile single-ion electrolyte with a Grotthuss-like Li conduction mechanism for dendrite-free Li metal batteries. *Energy Env. Sci.* **2019**, *12*, 2741−2750.

(20) Hou, T.; Fong, K. D.; Wang, J.; Persson, K. A. The solvation structure, transport properties and reduction behavior of carbonate-based electrolytes of lithium-ion batteries. *Chem. Sci.* **2021**, *12*, 14740−14751.

(21) Ringsby, A. J.; Fong, K. D.; Self, J.; Bergstrom, H. K.; McCloskey, B. D.; Persson, K. A. Transport Phenomena in Low Temperature Lithium-Ion Battery Electrolytes. *J. Electrochem. Soc.* **2021**, *168*, No. 080501.

(22) Giacobbe, C.; Lavigna, E.; Maspero, A.; Galli, S. Elucidating the CO_2 adsorption mechanisms in the triangular channels of the bis(pyrazolate) MOF $Fe_2(BPEB)_3$ by in situ synchrotron X-ray diffraction and molecular dynamics simulations. *J. Mater. Chem. A* **2017**, *5*, 16964−16975.

(23) Pillai, R. S.; Jobic, H.; Koza, M. M.; Nouar, F.; Serre, C.; Maurin, G.; Ramsahye, N. A. Diffusion of Carbon Dioxide and Nitrogen in the Small-Pore Titanium Bis(phosphonate) Metal-Organic Framework MIL-91 (Ti): A Combination of Quasielastic Neutron Scattering Measurements and Molecular Dynamics Simulations. *ChemPhysChem* **2017**, *18*, 2739−2746.

(24) Frenkel, D.; Smit, B. *Understanding Molecular Simulation: From Algorithms to Applications*; Elsevier: 2001; Vol. *1*.

(25) Zou, Z.; Ma, N.; Wang, A.; Ran, Y.; Song, T.; Jiao, Y.; Liu, J.; Zhou, H.; Shi, W.; He, B.; Wang, D.; Li, Y.; Avdeev, M.; Shi, S. Relationships Between Na^+ Distribution, Concerted Migration, and Diffusion Properties in Rhombohedral NASICON. *Adv. Energy Mater.* **2020**, *10*, 2001486.

(26) Zhang, Z.; Zou, Z.; Kaup, K.; Xiao, R.; Shi, S.; Avdeev, M.; Hu, Y. S.; Wang, D.; He, B.; Li, H.; Huang, X.; Nazar, L. F.; Chen, L. Correlated Migration Invokes Higher Na^+-Ion Conductivity in NaSICON-Type Solid Electrolytes. *Adv. Energy Mater.* **2019**, *9*, 1902373.

(27) Mehrer, H. *Diffusion in Solids: Fundamentals, Methods, Materials, Diffusion-Controlled Processes*; Springer-Verlag: Berlin Heidelberg, 2007; Vol. *155*.

(28) Borodin, O.; Self, J.; Persson, K. A.; Wang, C.; Xu, K. Uncharted Waters: Super-Concentrated Electrolytes. *Joule* **2020**, *4*, 69−100.

(29) Self, J.; Fong, K. D.; Persson, K. A. Transport in Super-concentrated $LiPF_6$ and $LiBF_4$/Propylene Carbonate Electrolytes. *ACS Energy Lett.* **2019**, *4*, 2843−2849.

(30) Ding, M. S.; Xu, K.; Zhang, S. S.; Amine, K.; Henriksen, G. L.; Jow, T. R. Change of Conductivity with Salt Content, Solvent Composition, and Temperature for Electrolytes of $LiPF_6$ in Ethylene Carbonate-Ethyl Methyl Carbonate. *J. Electrochem. Soc.* **2001**, *148*, A1196−A1204.

(31) Hubble, D.; Brown, D. E.; Zhao, Y.; Fang, C.; Lau, J.; McCloskey, B. D.; Liu, G. Liquid electrolyte development for low-temperature lithium-ion batteries. *Energy Env. Sci.* **2022**, *15*, 550−578.

(32) Goujon, L. J.; Khaldi, A.; Maziz, A.; Plesse, C.; Nguyen, G. T. M.; Aubert, P.-H.; Vidal, F.; Chevrot, C.; Teyssié, D. Flexible Solid Polymer Electrolytes Based on Nitrile Butadiene Rubber/Poly-(ethylene oxide) Interpenetrating Polymer Networks Containing Either LiTFSI or EMITFSI. *Macromolecules* **2011**, *44*, 9683−9691.

(33) Yang, K.; Zhou, G.; Xu, Q. The elasticity of MOFs under mechanical pressure. *RSC Adv.* **2016**, *6*, 37506−37514.

(34) Manuel Stephan, A. Review on gel polymer electrolytes for lithium batteries. *Eur. Polym. J.* **2006**, *42*, 21−42.

(35) Moreno, M.; Quijada, R.; Santa Ana, M. A.; Benavente, E.; Gomez-Romero, P.; González, G. Electrical and mechanical properties of poly(ethylene oxide)/intercalated clay polymer electrolyte. *Electrochim. Acta* **2011**, *58*, 112−118.

(36) Klongkan, S.; Pumchusak, J. Effects of Nano Alumina and Plasticizers on Morphology, Ionic Conductivity, Thermal and Mechanical Properties of $PEO-LiCF_3SO_3$ Solid Polymer Electrolyte. *Electrochim. Acta* **2015**, *161*, 171−176.

(37) Xue, Z.; He, D.; Xie, X. Poly(ethylene oxide)-based electrolytes for lithium-ion batteries. *J. Mater. Chem. A* **2015**, *3*, 19218−19253.

(38) Rosen, A. S.; Mian, M. R.; Islamoglu, T.; Chen, H.; Farha, O. K.; Notestein, J. M.; Snurr, R. Q. Tuning the Redox Activity of Metal-Organic Frameworks for Enhanced, Selective O_2 Binding: Design Rules and Ambient Temperature O_2 Chemisorption in a Cobalt-Triazolate Framework. *J. Am. Chem. Soc.* **2020**, *142*, 4317−4328.

(39) Rosen, A. S.; Iyer, S. M.; Ray, D.; Yao, Z.; Aspuru-Guzik, A.; Gagliardi, L.; Notestein, J. M.; Snurr, R. Q. Machine learning the quantum-chemical properties of metal−organic frameworks for accelerated materials discovery. *Matter* **2021**, *4*, 1578−1597.

(40) Lyu, H.; Ji, Z.; Wuttke, S.; Yaghi, O. M. Digital Reticular Chemistry. *Chem.* **2020**, *6*, 2219−2241.